



## Abstract

30

31 The steering principle of tropical cyclone motion has been applied to tropical  
32 cyclone forecast and research for nearly 100 years. Two fundamental questions  
33 remain unanswered. One is why the steering flow plays a dominant role in tropical  
34 cyclone motion and the other is when tropical cyclone motion deviates considerably  
35 from the steering. A high-resolution numerical experiment was conducted with the  
36 tropical cyclone in a typical large-scale monsoon trough over the western North  
37 Pacific. The simulated tropical cyclone experiences two eyewall replacement  
38 processes.

39 Based on the potential vorticity tendency (PVT) diagnostics, this study  
40 demonstrates that the conventional steering, which is calculated over a certain radius  
41 from the tropical cyclone center in the horizontal and a deep pressure layer in the  
42 vertical, plays a dominant role in tropical cyclone motion since the contributions from  
43 other processes are largely cancelled out due to the coherent structure of tropical  
44 cyclone circulation. Resulting from the asymmetric dynamics of the tropical cyclone  
45 inner core, the trochoidal motion around the mean tropical cyclone track cannot be  
46 accounted for by the conventional steering. The instantaneous tropical cyclone motion  
47 can considerably deviate from the conventional steering that approximately accounts  
48 for the combined effect of the contribution of the advection of the symmetric potential  
49 vorticity component by the asymmetric flow and the contribution from the advection  
50 of the wavenumber-one potential vorticity component by the symmetric flow.

51

52 **1. Introduction**

53 The environmental steering principle has been applied to tropical cyclone track  
54 forecasting for nearly 100 years (Fujiwara and Sekiguchi 1919; Bowie 1922), which  
55 states that a tropical cyclone tends to follow the large-scale flow in which it is  
56 embedded. Such a steering concept has been extended to include the beta drift (also  
57 called secondary steering) that arises mainly from the interaction between tropical  
58 cyclone circulation and the planetary vorticity gradient (Holland 1983; Chan 1984;  
59 Chan and Williams 1987; Fiorino and Elsberry 1989; Carr and Elsberry 1990; and  
60 Wang and Li 1992; Wang and Holland 1996a). The steering flow is usually calculated  
61 over a certain radius from the tropical cyclone center in the horizontal and a deep  
62 pressure layer in the vertical (Dong and Neumann 1986; Velden and Leslie 1991;  
63 Franklin et al. 1996). For convenience, here we call it the conventional steering flow.  
64 As a rule of thumb, the conventional steering flow has been extensively used in  
65 tropical cyclone track forecasting and understanding of tropical cyclone motion (e.g.,  
66 Simpson 1948; Riehl and Burgner 1950; Chan and Gray 1982; Fiorino and Elsberry  
67 1989; Neumann 1993; Wu and Emanuel 1995a, b; Wang and Holland 1996b, c; Wu et  
68 al. 2011a; Wu et al. 2011b). Given complicated interactions between tropical cyclone  
69 circulation and its environment, tropical cyclone motion should be not like a leaf  
70 being steered only by the currents in the stream. Therefore, two fundamental issues  
71 are still remaining on the steering principle. First, why can the conventional steering  
72 plays a dominant role in tropical cyclone motion? Second, when may tropical cyclone  
73 motion deviate considerably from the conventional steering?

74       The potential vorticity tendency (PVT) paradigm for tropical cyclone motion was  
75       proposed by Wu and Wang (2000), in which a tropical cyclone tends to move to the  
76       region of the PVT maximum. In other words, tropical cyclone motion is completely  
77       determined by the azimuthal wavenumber-one component of PVT and all of the  
78       factors that contribute to the azimuthal wavenumber-one component of PVT play a  
79       potential role in tropical cyclone motion. The contributions of individual factors can  
80       be quantified through the PVT diagnosis and the steering effect is one of the factors  
81       (Wu and Wang 2000). Wu and Wang (2000, 2001a) evaluated the PVT approach using  
82       the output of idealized numerical experiments with a coarse spacing of 25 km and  
83       understood the vertical coupling of tropical cyclone circulation under the influence of  
84       vertical wind shear. Wu and Wang (2001b) found that convective heating can affect  
85       tropical cyclone motion by the heating-induced flow and the positive PVT that is  
86       directly generated by convective heating.

87       The PVT paradigm was further verified by Chan et al. (2002). The observational  
88       analysis indicated that the potential vorticity advection process is generally dominant  
89       in tropical cyclone motion without much change in direction or speed while the  
90       contribution by diabatic heating is usually less important. An interesting finding in the  
91       study is that the contribution of diabatic heating becomes important for irregular  
92       tropical cyclone motion, suggesting that track oscillations as well as irregular track  
93       changes may be explained by changes in the convection pattern. The PVT approach  
94       has been used in understanding tropical cyclone motion in the presence of the effects  
95       of land surface friction, river deltas, coastal lines, mountains, islands, cloud-radiative

96 processes and sea surface pressure gradients (e.g., Wong and Chan 2006; Yu et al.  
97 2007; Fovell et al. 2010; Hsu et al. 2013; Wang et al. 2013; Choi et al. 2013).

98 As we know, the coarse resolution of the numerical experiment in Wu and Wang  
99 (2000) was unable to resolve the eyewall structure and tropical cyclone rainbands,  
100 which may affect tropical cyclone motion (Holland and Lander 1993; Nolan et al.  
101 2001; Oda et al. 2006; Hong and Chang 2009). Under the PVT paradigm, in this study  
102 we use the output from a high-resolution numerical experiment to address the  
103 aforementioned two fundamental issues that are important to understanding tropical  
104 cyclone motion. The numerical experiment was conducted with the advanced research  
105 version of the Weather Research and Forecast (ARW-WRF) model. In particular, an  
106 initially symmetric baroclinic vortex is embedded in the low-frequency atmospheric  
107 circulation of Typhoon Matsa (2005) to simulate tropical cyclone motion in a realistic  
108 large-scale environment. For simplicity, the present study focuses on the numerical  
109 experiment without the influences of land surface and topography.

## 110 **2. The output of the numerical experiment**

111 The numerical experiment conducted with the WRF model (version 2.2) in this  
112 study contains a coarsest domain centered at 30.0°N, 132.5°E and four two-way  
113 interactive domains. In order to better simulate the tropical cyclone rainbands and  
114 eyewall structure, the horizontal resolutions are 27, 9, 3, 1, 1/3 km, respectively. The  
115 three innermost domains move with the tropical cyclone (Fig. 1). The model consists  
116 of 40 vertical levels with a top of 50 hPa. The WRF single-moment 3-class scheme  
117 and the Kain-Fritsch cumulus parameterization scheme (Kain and Fritsch 1993) are

118 used in the outmost domain. The WRF single-moment 6-class scheme (Hong and Lim  
119 2006) and no cumulus parameterization scheme are used in the four inner domains.  
120 The other model physics options are the Rapid Radiative Transfer Model (RRTM)  
121 longwave radiation scheme (Mlaewe et al. 1997), the Dudhia shortwave radiation  
122 scheme (Dudhia 1989), and the Yonsei University scheme for planetary boundary  
123 layer parameterization (Noh et al. 2003).

124 The National Centers for Environmental Prediction (NCEP) Final (FNL)  
125 Operational Global Analysis data with resolution of  $1.0^\circ \times 1.0^\circ$  at every 6 h were used  
126 for deriving the large-scale background with a 20-day low-pass Lanczos filter  
127 (Duchon 1979). The low-frequency fields were taken from those of Typhoon Matsa  
128 (2005) from 0000 UTC 5 August to 0000 UTC 9 August 2005. At 0000 UTC 5 August,  
129 the typhoon was located to the northeast of Taiwan Island with the maximum surface  
130 wind of  $45 \text{ m s}^{-1}$ . During the following three days, Matsa moved northwestward in the  
131 monsoon trough and made landfall on mainland China at 1940 UTC 5 August. The  
132 sea surface temperature is spatially uniform being  $29^\circ\text{C}$ . The analysis nudging for the  
133 wind components above the lower boundary layer is used in the coarsest domain to  
134 maintain the large-scale patterns with a nudging coefficient of  $1.5 \times 10^{-4} \text{ s}^{-1}$ .

135 A symmetric vortex is initially embedded at  $25.4^\circ\text{N}$ ,  $123.0^\circ\text{E}$  (Matsa's center) in  
136 the background (Fig. 1). The vortex was spun up for 18 hours on an f-plane without  
137 environmental flows to make it relatively consistent with the WRF model dynamics  
138 and physics. Considering several hours of the initial spin-up, here we focus only on  
139 the 72-hour period from 6 h to 78 h with the output at one-hour intervals. The

140 simulated tropical cyclone takes a northwest north track (Fig. 1), generally similar to  
141 that of Typhoon Matsa (2005). The evolution of tropical cyclone intensity is shown in  
142 Figure 2.

143 Figure 3 shows the simulated wind and radar reflectivity fields at 700 hPa. The  
144 vertical wind shear, which is calculated between 200 hPa and 850 hPa over a radius of  
145 500 km from the tropical cyclone center, is also plotted in the figure. The tropical  
146 cyclone center is defined as the geometric center of the circle on which the azimuthal  
147 mean tangential wind speed reaches a maximum (Wu et al. 2006). We use a  
148 variational method to determine the tropical cyclone center each hour at each level.  
149 Different definitions of the tropical cyclone center are also used and it is found that  
150 fluctuations in tropical cyclone translation do not depend on the specific definition of  
151 the tropical cyclone center. At 24 h (Fig. 3a), the vertical wind shear is more than 10  
152  $\text{m s}^{-1}$ . The eyewall is open to the southwest and strong eyewall convection occurs  
153 mainly on the downshear left side (Frank and Ritchie 2001). The rainbands simulated  
154 in the inner most domain exhibit apparent cellular structures (Houze 2010), mostly on  
155 the eastern side. The eyewall replacement cycle (ERC), which is important for  
156 tropical cyclone intensity change (Wu et al. 2012; Huang et al. 2012), is simulated in  
157 this numerical experiment. At 48 h (Fig. 3b), the vertical wind shear is weaker and the  
158 tropical cyclone undergoes an ERC. At 72 h (Fig. 3c), the outer eyewall just forms  
159 while the inner one is breaking during the second ERC. Figure 3 suggests that the  
160 simulated tropical cyclone has a structure similar to a typical observed one, especially  
161 in the inner core region.

162 Two eyewall replacement processes, which may affect tropical cyclone motion  
 163 (Oda et al. 2006; Hong and Chang 2009), can be further shown in Figure 4. The  
 164 evolution of the azimuthal mean component of the 700-hPa wind in the 9-km domain  
 165 indicates the eyewall replacement processes around 42 h and 68 h, respectively.  
 166 During the first eyewall replacement, for example, the wind starts to intensify outside  
 167 the eyewall around 36 h, in agreement with previous numerical studies (Wu et al.  
 168 2012; Huang et al. 2012). The radius of maximum wind is located at about 40 km  
 169 after the 6-h spin-up and decreases to about 30 km at 42 h. We also conducted a  
 170 similar sensitivity experiment without the sub-kilometer domain. The tropical cyclone  
 171 track in the experiment is generally similar to that in the sub-kilometer simulation, but  
 172 no eyewall replacement cycle can be observed in the sensitivity experiment.

### 173 **3. Dominant role of the conventional steering**

174 The relationship between PVT and tropical cyclone motion can be written as (Wu  
 175 and Wang 2000)

$$176 \quad \left(\frac{\partial P_1}{\partial t}\right)_f = \left(\frac{\partial P_1}{\partial t}\right)_m - \mathbf{C} \cdot \nabla P_s, \quad (1)$$

177 Where subscripts  $m$  and  $f$  indicate, respectively, the moving and fixed reference frames  
 178 and  $\mathbf{C}$  is the velocity of the reference frame that moves with the tropical cyclone. In  
 179 other words,  $\mathbf{C}$  is the velocity of tropical cyclone motion, which can vary in the  
 180 vertical.  $P_l$  and  $P_s$  are the azimuthal wavenumber-one and symmetric components of  
 181 potential vorticity with respect to the storm center. It can be seen that the PVT  
 182 generated in the fixed reference frame (the term on the left hand side) is provided for  
 183 the development of the wavenumber one component (the first term on the right hand



184 side) and for tropical cyclone motion (the second term on the right hand side). The  
 185 first term on the right hand side of Eq. (1) was neglected in Wu and Wang (2000), but  
 186 we retain it in this study. The term can be calculated with the two-hour change of the  
 187 wavenumber one component in the frame that moves with the tropical cyclone center.

188 The PVT generated in the fixed reference frame can be calculated with the PVT  
 189 equation in  $p$ -coordinates as

$$190 \quad \frac{\partial P}{\partial t} = -\mathbf{V} \cdot \nabla P - \omega \frac{\partial P}{\partial p} - g \nabla_3 \cdot \left( -\frac{Q}{c_p \pi} \mathbf{q} + \nabla \theta \times \mathbf{F} \right), \quad (2)$$

191 Where  $P$ ,  $\mathbf{V}$  and  $\boldsymbol{\omega}$  are potential vorticity, horizontal and vertical components of the  
 192 wind velocity, respectively. Eq. (2) contains horizontal advection (HA), vertical  
 193 advection (VA), diabatic heating (DH) and friction (FR) terms on the right hand side.  
 194  $Q$ ,  $\theta$ ,  $\mathbf{q}$  and  $\mathbf{F}$  are diabatic heating rate, potential temperature, absolute vorticity and  
 195 friction, while  $g$ ,  $c_p$  and  $\pi$  are the gravitational acceleration, the specific heat of dry air  
 196 at constant pressure and the Exner function.  $\nabla_3$  and  $\nabla$  denote the three and two  
 197 dimensional gradient operators.

198 Following Wu and Wang (2000), a least square method is used to estimate the  
 199 velocity of tropical cyclone motion ( $\mathbf{C}$ ) in Eq. (1). The translation velocity is also  
 200 calculated with the hourly positions of the tropical cyclone center. For convenience,  
 201 the tropical cyclone motion estimated with the PVT diagnostic approach and with the  
 202 center position is referred to as the PVT velocity and the tropical cyclone velocity,  
 203 respectively, in the following discussion. In the PVT approach, we find that the  
 204 estimated tropical cyclone motion is not much sensitive to the size of the calculation  
 205 domain. As we know, however, determination of the conventional steering flow for a

206 given tropical cyclone is not unique and depends on the size of the calculation domain  
207 (Wang et al. 1998). Here we select the calculation domain to minimize the difference  
208 between the tropical cyclone speed and the conventional steering flow. After a series  
209 of tests, we find that such a minimum can be reached when the 270-km radius is used.  
210 This is consistent with the analysis of the airborne Doppler radar data in Marks et al.  
211 (1992) and Franklin et al. (1996). The analysis indicated that tropical cyclone motion  
212 was best correlated with the depth-mean flow averaged over the inner region within  $3^\circ$   
213 latitudes. Note that the PVT, tropical cyclone and steering velocities are calculated at  
214 each level and then the depth-mean ones are averaged over the layer between 850-300  
215 hPa.

216 Figure 5a shows the time series of the magnitudes of the tropical cyclone velocity  
217 (black), the PVT velocity (blue) and the conventional steering (red). Note that the  
218 PVT velocity and the conventional steering are instantaneous, whereas the tropical  
219 cyclone velocity is calculated based on the two-hour difference of the center position.  
220 For consistence, a three-point running mean is applied to the PVT speed and the  
221 conventional steering. These magnitudes generally increase as the tropical cyclone  
222 takes a northwest north track. The mean speeds calculated from the PVT approach  
223 and the center positions are  $2.86 \text{ m s}^{-1}$  and  $2.75 \text{ m s}^{-1}$  over the 72-h period. Compared  
224 to the tropical cyclone speed, the root-mean-square error (RMSE) of the PVT speed is  
225  $0.22 \text{ m s}^{-1}$ , only accounting for 8% of the tropical cyclone speed.

226 Figures 5b and 5c further display the zonal and meridional components of the  
227 tropical cyclone velocity (black), the PVT velocity (blue) and the conventional

228 steering (red). While the westward component fluctuates about the mean zonal  
229 tropical cyclone (PVT) speed of  $-1.0 \text{ m s}^{-1}$ , the northward component generally  
230 increases with time. Figure 5 clearly indicates that the translation velocity of the  
231 tropical cyclone can be well estimated with the PVT approach.

232 The environmental and secondary steering flows are indistinctly referred to the  
233 conventional steering flow in this study. The conventional steering shown in Fig. 5 is  
234 averaged over the same radius (270 km) and the 850-300 hPa layer, as used in the  
235 calculation of the PVT speed. The 72-h mean magnitudes of the tropical cyclone  
236 velocity and the conventional steering are  $2.86 \text{ m s}^{-1}$  and  $2.87 \text{ m s}^{-1}$ , respectively, only  
237 with a difference of  $6.7^\circ$  in the motion direction. We also calculated the  
238 root-mean-square-error (RMSE) of the conventional steering averaged over various  
239 time periods with the tropical cyclone speed (Fig. 6). The RMSE of the magnitude  
240 decreases with the increasing average period, generally less than 9% of the translation  
241 speed of the tropical cyclone. The difference in direction also decreases with the  
242 increasing average period within 9-11 degrees. Considering uncertainties in  
243 determining tropical cyclone centers and calculating the steering, we conclude that the  
244 conventional steering plays a dominant role in tropical cyclone motion. However,  
245 Figure 5 indicates that the instantaneous tropical cyclone motion can considerably  
246 deviate from the conventional steering. The conventional steering cannot account for  
247 the fluctuations in tropical cyclone motion, which will be further discussed in Section  
248 5.

#### 249 **4. Contributions of individual processes**

250 The individual contributions of various terms in the PVT equation to tropical  
251 cyclone motion can also be estimated with Eq. (1), as shown by Wu and Wang (2000).  
252 In this study, the contribution of the friction (FR) term is calculated as the residual of  
253 the PVT equation. Figure 7 shows the individual contributions of the terms in the  
254 PVT equation to tropical cyclone motion. While the contribution of the HA term plays  
255 a dominant role (Fig. 7c), the figure exhibits considerable fluctuations, suggesting that  
256 the contributions of the DH and VA terms tend to cancel each other (Figs. 7a and 7b).  
257 Here we discuss the contribution of each term in the PVT equation to understand the  
258 dominant role of the conventional steering in tropical cyclone motion.

#### 259 **a. Horizontal advection**

260 As discussed in Wu and Wang (2001b), the HA term in the PVT equation can be  
261 approximately written as:  $-\mathbf{V}_1 \cdot \nabla \mathbf{P}_s - \mathbf{V}_s \cdot \nabla \mathbf{P}_1$ , where  $\mathbf{V}_s$  is the symmetric  
262 component of the tangential wind and  $\mathbf{V}_1$  is the wavenumber-one component of the  
263 asymmetric wind. The first term (HA1) represents the advection of the symmetric  
264 potential vorticity component by the asymmetric flow. The second term is the  
265 advection of the wavenumber-one potential vorticity component by the symmetric  
266 flow (HA2).

267 The contribution of the HA1 term is literally the steering effect, but it is not the  
268 conventional steering that is calculated as the velocity of the mean wind averaged  
269 over 300-850 hPa within the radius of 270 km from the tropical cyclone center in this  
270 study. Wu and Wang (2001a) pointed out that the steering effect in the HA1 term is

271 associated also with the gradient of the symmetric potential vorticity component,  
272 which make its contribution be confined to the inner region of tropical cyclones.

273 Figure 8 shows the contributions of the HA1 and HA2 terms, which exhibit  
274 considerable fluctuations with time. The contribution of HA and the conventional  
275 steering are also plotted. For clarity, the conventional steering is removed from the  
276 contribution of HA1 (i.e. HA1'). The 72-hour mean difference between the  
277 contribution of HA1 and the conventional steering is  $-1.25 \text{ m s}^{-1}$  in the zonal  
278 component and  $1.62 \text{ m s}^{-1}$  in the meridional component, suggesting that the  
279 contribution of the HA1 term is considerably different from the conventional steering.  
280 In fact, the contributions of the HA1 and HA2 terms are highly anticorrelated. The  
281 correlations for the zonal and meridional components are  $-0.82$  and  $-0.80$ , respectively.  
282 The negative correlations suggest the cancellation between the contributions of the  
283 HA1 and HA2 terms. As a result, the combined effect of the HA1 and HA2 terms can  
284 actually account for the effect of the conventional steering except the short-time  
285 fluctuations, as shown in Fig. 8. It is interesting to note that the contributions of the  
286 HA1 and HA2 terms increase in magnitude during the two eyewall replacement  
287 processes around 42 h and 68 h, suggesting that the tropical cyclone motion  
288 considerably deviates from the steering of the asymmetric flow during eyewall  
289 replacement.

290 The cancellation between the contributions of the HA1 and HA2 terms arises  
291 from the interaction between the symmetric and wavenumber-one components of the  
292 tropical cyclone circulation. As an example, Figure 9a shows HA1 and the

293 wavenumber-one components of potential vorticity (contours) and winds at 700 hPa  
294 after 18 hours of the integration. The positive (negative) anomalies of potential  
295 vorticity are nearly collocated with the cyclonic (anticyclonic) circulation. Since the  
296 potential vorticity in the inner core is generally elevated, the advection of the  
297 symmetric potential vorticity component by the flows between the cyclonic and  
298 anticyclonic circulations leads to the maximum (minimum) HA1 in the exit (entrance)  
299 of the flows between the cyclonic and anticyclonic circulation. On the other hand, the  
300 advection of the wavenumber-one component of potential vorticity by the symmetric  
301 cyclonic flow leads to the maximum HA2 in the entrance and the minimum HA1 in  
302 the exit (Fig. 9b). Although the contributions of the HA1 and HA2 terms can fluctuate  
303 with a magnitude of about  $4 \text{ m s}^{-1}$  (Fig. 8), their combined effect shows only  
304 small-amplitude fluctuations in the tropical cyclone motion. The short-time  
305 fluctuations will be discussed in the next section.

#### 306 **b. Contributions of diabatic heating and vertical advection**

307 Some individual contributions in Figs. 7a and 7b are statistically correlated. For  
308 example, the zonal contribution of the HA term is negatively correlated with that of  
309 the DH term with a coefficient of -0.44, and the meridional contribution of the HA  
310 term is negatively correlated with that of the VA terms with a coefficient of -0.54.  
311 The correlation coefficients pass the significance test at the 95% confidence level. It is  
312 suggested that the contributions of individual terms can partially cancel each other  
313 due to the coherent structure of the tropical cyclone.

314 We first discuss the contribution of the VA term. The VA contains two primary  
315 terms: the advection of the symmetric component of potential vorticity by the  
316 wavenumber-one component of vertical motion (VA1) and wavenumber-one  
317 component of potential vorticity by the symmetric component of vertical motion  
318 (VA2). Our examination indicates that the contribution of the VA term is dominated  
319 by that of VA1. That is, the direction of the contribution of the VA term is determined  
320 by the orientation of the wavenumber-one component of vertical motion. Figure 10  
321 shows the wavenumber-one components of the 500-hPa vertical motion, 700-hPa  
322 winds relative to tropical cyclone motion, and 500-hPa heating rate after 18 hours of  
323 integration. We can see that the upward (downward) motion generally occurs in the  
324 entrance (exit) region of the 700-hPa winds. Bender (1997) found that vorticity  
325 stretching and compression is closely associated with the vorticity advection due to  
326 the relative flow (difference between the wavenumber-one flow and the TC motion),  
327 but Riemer (2016) recently argued that Bender's mechanism did not work in his  
328 idealized experiment. We find that the contribution of the HA term is indeed  
329 significantly correlated with those of the VA and DH terms, suggesting the  
330 relationship between the vertical motion (diabatic heating) and the relative flow.

331 The contribution of diabatic heating results mainly from  $-\mathbf{q}_s \cdot \nabla_3 h_1$ , where  $\mathbf{q}_s$   
332 is the symmetric component of the absolute vorticity,  $\nabla_3$  the three-dimensional  
333 gradient operator,  $h_1$  the wavenumber-one component of diabatic heating rate. Since  
334 the absolute vorticity is dominated by the vertical component of relative vorticity and  
335 diabatic heating rate reaches its maximum in the middle troposphere, it is conceivable

336 that the contribution of diabatic heating should cancel each other in the low and upper  
337 troposphere. Figure 11 shows the contribution of diabatic heating at 700 hPa and 400  
338 hPa. The correlation between 700 hPa and 400 hPa is -0.68 in the zonal direction and  
339 -0.67 in the meridional direction.

## 340 **5. Trochoidal motion**

341 As shown in Fig. 5, the tropical cyclone motion exhibits considerable fluctuations.  
342 In an instant, the steering can significantly deviate from the tropical cyclone motion.  
343 At 60 h, for example, the zonal steering is  $-0.55 \text{ m s}^{-1}$ , about one third of the zonal  
344 motion of the tropical cyclone ( $-1.42 \text{ m s}^{-1}$ ); The meridional steering is  $2.71 \text{ m s}^{-1}$ ,  
345 slower than the meridional motion of the tropical cyclone ( $3.05 \text{ m s}^{-1}$ ). The deviation  
346 from the tropical cyclone motion is  $13.5^\circ$  in the direction and 18% in the magnitude.  
347 It is clear that the instantaneous velocity of tropical cyclone motion can considerably  
348 deviate from the conventional steering.

349 Based on radar data and satellite images, many studies documented the oscillation  
350 of a tropical cyclone track with respect to its mean motion vector (e. g., Jordan and  
351 Stowell 1955; Lawrence and Mayfield 1977; Muramatsu 1986; Itano et al. 2002;  
352 Hong and Chang 2005). The periods of track oscillations range less than an hour to a  
353 few days (Holland and Lander 1993). In this study, the small-scale oscillation with  
354 amplitudes of that comparable to the eye size and periods of several hours is referred  
355 to as the trochoidal motion of the tropical cyclone center. Willoughby (1988) showed  
356 that a pair of rotating mass and sink source could lead to trochoidal motion with  
357 periods ranging from 2-10 hours. Flatau and Stevens (1993) argued that



358 wavenumber-one instabilities in the outflow layer of tropical cyclones could cause  
359 trochoidal motion. Nolan et al. (2001) found that the small-amplitude trochoidal  
360 motion is associated with the instability of the wavenumber-one component of  
361 tropical cyclone circulation due to the presence of the low-vorticity eye. The  
362 instability in their three-dimensional simulation with a baroclinic vortex quickly led to  
363 substantial inner-core vorticity redistribution and mixing, displacing the vortex center  
364 that rotates around the vortex core. Our spectral analysis indicates two peaks of the  
365 fluctuations of the tropical cyclone motion centered at 5 hours and 9 hours (Figure not  
366 shown), suggesting that the trochoidal motion is simulated in our high-resolution  
367 numerical simulation.

368 Figure 12 shows the oscillation of the tropical cyclone track with respect to the  
369 9-hour running mean track for the periods 6-18 h and 59-70 h. We can see that the  
370 displacement from the mean track is usually less than 6 km with a period of several  
371 hours in this study. This displacement is less than the size of the tropical cyclone eye.  
372 In general, the tropical cyclone center rotates cyclonically relative to the mean track  
373 position, in agreement with previous observational and numerical studies (Lawrence  
374 and Mayfield 1977; Muramatsu 1986; Itano et al. 2002; Willoughby 1988; Nolan et al.  
375 2001). In association with the trochoidal motion of the tropical cyclone center, as  
376 suggested by Nolan et al. (2001), substantial potential vorticity redistribution and  
377 mixing can be observed in the inner core region (Fig. 13). During the period of 13-18  
378 hours, the tropical cyclone eye generally looks like a triangle, but the orientation of

379 the triangle changes rapidly, suggesting the potential vorticity redistribution and  
380 mixing in the eye.

381 The trochoidal motion is well indicated in the translation speed estimated with the  
382 PVT approach. Figure 14a shows the fluctuations of tropical cyclone speed, the PVT  
383 speed, and the difference between the tropical cyclone speed and the conventional  
384 steering, in which the 9-hour running mean has been removed. We can see that the  
385 fluctuations of tropical cyclone motion are well represented in the PVT speed.  
386 Moreover, the consistence between the fluctuations of tropical cyclone motion and  
387 those with the conventional steering removed suggests that the small-amplitude  
388 oscillation of the tropical cyclone motion cannot be accounted for by the conventional  
389 steering. Figure 14b further compares the time series of tropical cyclone motion  
390 relative to the conventional steering with the time series of the contribution of the HA  
391 term relative to the conventional steering. The two time series are correlated with a  
392 coefficient of 0.60. We can see that the contribution of the HA term plays an  
393 important role in the fluctuations. Since the non-steering effect can well account for  
394 the fluctuations (Fig. 14a), Figure 14b suggests that the VA and DH tend to reduce the  
395 magnitude of the fluctuations.

## 396 **6. Summary**

397 In this study, we addressed two fundamental questions regarding the steering  
398 principle that has been widely applied to tropical cyclone forecast and research for  
399 about a century (Fujiwara and Sekiguchi 1919; Bowie 1922). One is why the  
400 conventional steering plays a dominant role in tropical cyclone motion and the other

401 is when tropical cyclone motion deviates considerably from the steering. The PVT  
402 diagnosis approach proposed by Wu and Wang (2000) is used with the output from a  
403 high-resolution numerical experiment. It is found that the PVT approach can well  
404 estimate tropical cyclone motion, including the small-amplitude trochoidal motion  
405 relative to the mean tropical cyclone track.

406       The effect of the conventional steering flow that is averaged over a certain radius  
407 from the tropical cyclone center and a deep pressure layer (e.g., 850-300 hPa) actually  
408 represents the combined contribution from both of the advection of the symmetric  
409 potential vorticity component by the asymmetric flow (HA1) and the advection of the  
410 wavenumber-one potential vorticity component by the symmetric flow (HA2),  
411 although the contribution of the HA1 term is literally the effect of steering (Wu and  
412 Wang 2001a, 2001b). The conventional steering generally plays a dominant role in  
413 tropical cyclone motion since the contributions from other processes are largely  
414 cancelled out due to the coherent structure of tropical cyclone circulation.

415       The trochoidal motion of the tropical cyclone center is simulated in the numerical  
416 experiment with amplitudes smaller than the eye radius and periods of several hours.  
417 The tropical cyclone center rotates cyclonically around the mean track, in agreement  
418 with previous observational and numerical studies (Lawrence and Mayfield 1977;  
419 Muramatsu 1986; Itano et al. 2002; Willoughby 1988; Nolan et al. 2001). It is found  
420 that the small-amplitude trochoidal motion cannot be accounted for by the effect of  
421 the conventional steering although the contribution of the HA term plays an important  
422 role in the fluctuations. In agreement with previous studies (Willoughby 1988; Nolan

423 et al. 2001), we suggest that the small-amplitude trochoidal motion results from the  
424 asymmetric dynamics of the tropical cyclone inner core. It is also found that the  
425 instantaneous speed of tropical cyclone motion can considerably deviate from the  
426 conventional steering, while the latter better represents tropical cyclone motion when  
427 averaged over a reasonable time period.

428 **Acknowledgements.** Many thanks go to Dr. Christopher W. Landsea of the National  
429 Hurricane Center for providing us the early references on the steering principle. This  
430 research was jointly supported by the National Basic Research Program of China  
431 (2013CB430103, 2015CB452803), the National Natural Science Foundation of China  
432 (Grant No. 41275093), and the project of the specially-appointed professorship of  
433 Jiangsu Province. We appreciate Dr. C.-C. Wu and two anonymous reviewers for their  
434 constructive comments.

435

436 **References:**

437 Bender, M. A., 1997: The effect of relative flow on the asymmetric structure in the  
438 interior of hurricanes. *J. Atmos. Sci.*, **54**, 703–724.

439 Bowie, E. H., 1922: Formation and movement of West Indian hurricanes. *Mon. Wea.*  
440 *Rev.*, **50**, 173-179.

441 Carr, L. E., and R. L. Elsberry, 1990: Observational evidence for predictions of  
442 tropical cyclone propagation relative to steering. *J. Atmos. Sci.*, **47**, 542–546.

443 Chan, J. C. –L., F. M. F. Ko, and Y. M. Lei, 2002: Relationship between potential  
444 vorticity tendency and tropical cyclone motion. *J. Atmos. Sci.*, **59**, 1317-1336.

445 Chan, J. C. -L., and W. M. Gray, 1982: Tropical cyclone motion and surrounding flow  
446 relationship. *Mon. Wea. Rev.*, **110**, 1354-1374.

447 Chan, J. C. -L., 1984: An observational study of physical processes responsible for  
448 tropical cyclone motion. *J. Atmos. Sci.*, **41**, 1036-1048.

449 Chan, J. C-L., and R. T. Williams, 1987: Analytical and numerical studies of  
450 beta-effect in tropical cyclone motion. Part I: Zero mean flow. *J. Atmos. Sci.*, **44**,  
451 1257–1265.

452 Choi, Y., K.-S. Yun, K.-J. Ha, K.-Y. Kim, S.-J. Yoon, J.-C.-L. Chan, 2013: Effects of  
453 Asymmetric SST Distribution on Straight-Moving Typhoon Ewiniar (2006) and  
454 Recurving Typhoon Maemi (2003). *Mon. Wea. Rev.* **141**, 3950-3967.

455 Duchon, C. E., 1979: Lanczos filtering in one and two dimensions. *J. Appl. Meteor.*, **18**,  
456 1016–1022.

457 Dudhia, J., 1989: Numerical study of convection observed during the winter monsoon  
458 experiment using a mesoscale two-dimensional model. *J. Atmos. Sci.*, **46**,  
459 3077-3107.

460 Flatau, M., W. H. Schubert, and D. E. Stevens, 1994: The role of baroclinic processes  
461 in tropical cyclone motion: The influence of vertical tilt. *J. Atmos. Sci.*, **51**,  
462 2589–2601.

463 Fiorino, M., and R. L. Elsberry, 1989: Some aspects of vortex structure related to  
464 tropical cyclone motion. *J. Atmos. Sci.*, **46**, 975-990.

465 Fovell, R. G., K. L. Corbosiero, A. Seifert, and K.-N. Liou, 2010: Impact of  
466 cloud-radiative processes on hurricane track, *Geophys. Res. Lett.*, **37**, L07808,

467 doi:10.1029/2010GL042691.

468 Frank, W., and E. A. Ritchie, 2001: Effects of vertical wind shear on the intensity and  
469 structure of numerically simulated hurricanes. *Mon. Wea. Rev.*, **129**, 2249–2269.

470 Franklin, J. L., S. E. Feuer, J. Kaplan, and S. D. Aberson, 1996: Tropical cyclone  
471 motion and surrounding flow relationship: Searching for beta gyres in Omega  
472 dropwindsonde datasets. *Mon. Wea. Rev.*, **124**, 64–84.

473 Fujiwhara, S., and K. Sekiguchi, 1919: Estimated 300 m isobars and the weather of  
474 Japan. *J. Meteor. Soc. Japan*, **38**, 254-259 (in Japanese).

475 Holland, G. J., 1983: Tropical cyclone motion: Environmental interaction plus a beta  
476 effect. *J. Atmos. Sci.*, **40**, 328–342.

477 Houze, R.A., 2010: Clouds in tropical cyclones. *Mon. Wea. Rev.*, **138**, 293–344.

478 Hsu, L.-H., Hung-Chi Kuo, Robert G. Fovell, 2013: On the Geographic Asymmetry  
479 of Typhoon Translation Speed across the Mountainous Island of Taiwan. *J.*  
480 *Atmos. Sci.* **70**, 1006-1022.

481 Huang, Y.-H., M. T. Montgomery, and C.-C. Wu, 2012: Concentric eyewall  
482 formation in Typhoon Sinlaku (2008) – Part II: Axisymmetric dynamical  
483 processes. *J. Atmos. Sci.*, **69**, 662-674.

484 Itano, T., G. Naito, and M. Oda, 2002: Analysis of elliptical eye of Typhoon Herb  
485 (T9609) (in Japanese with English abstract). *Sci. Eng. Rep. Natl. Def. Acad.*, **39**,  
486 9–17.

487 Kain, J. S., and J. M. Fritch, 1993: Convective parameterization for mesoscale models:  
488 the Kain-Fritch scheme. The representation of cumulus convection in numerical

489 models. *Meteorological Monographs*, **46**, 165-170.

490 Lawrence, M. B., and B. M. Mayfield, 1977: Satellite observations of trochoidal  
491 motion during Hurricane Belle 1976. *Mon. Wea. Rev.*, **105**, 1458–1461.

492 Marks, F. D., Jr., R. A. Houze, Jr., and J. F. Gamache, 1992: Dual-aircraft  
493 investigation of the inner core of Hurricane Norbert. Part I: Kinematic structure.  
494 *J. Atmos. Sci.*, **49**, 919–942.

495 Mlawer, E. J., S. J. Taobman, P. D. Brown, M. J. Iacono, and S. A. Clough, 1997:  
496 Radiative transfer for inhomogeneous atmosphere: RRTM, a validated  
497 correlated-k model for the longwave. *J. Geophys. Res.*, **102**, 16663-16682.

498 Muramatsu, T., 1986: Trochoidal motion of the eye of Typhoon 8019. *J. Meteor. Soc.*  
499 *Japan*, **64**, 259–272.

500 Noh, Y., W. G. Cheon, S.-Y. Hong, and S. Raasch, 2003: Improvement of the  
501 K-profile model for the planetary boundary layer based on large eddy simulation  
502 data. *Bound.-Layer Meteor.*, **107**, 401-427.

503 Neumann, C. J., 1993: Global overview. *Global Guide to Tropical Cyclone*  
504 *Forecasting*, World Meteor. Org., 1.1–1.56.

505 Nolan, D. S., M. T. Montgomery, and L. D. Grasso, 2001: The wavenumber-one  
506 instability and trochoidal motion of hurricane-like vortices. *J. Atmos. Sci.*, **58**,  
507 3243–3270.

508 Riehl, H., and N. M. Burgner, 1950: Further studies on the movement and formation  
509 of hurricanes and their forecasting. *Bull. Amer. Meteor. Soc.*, **31**, 244–253.

510 Riemer, M., 2016: Meso- $\beta$ -scale environment for the stationary band complex of

511 vertically-sheared tropical cyclones. *Q. J. R. Meteorol. Soc.*, **142**, 2442–2451.

512 Simpson, R. H., 1946: On the movement of tropical cyclones. *Trans. Amer. Geophys.*  
513 *Union*, **27**, 641-655.

514 Velden, C. S., and L. M. Leslie, 1991: The basic relationship between tropical cyclone  
515 intensity and the depth of the environmental steering layer in the Australian  
516 region. *Weather and Forecasting*, **6**, 244-253.

517 Wang, B., and X. Li, 1992: The beta drift of three-dimensional vortices: A numerical  
518 study. *Mon. Wea. Rev.*, **120**, 579–593.

519 Wang, B., R. L. Elsberry, Y. Wang, and L. Wu, 1998: Dynamics of tropical cyclone  
520 motion: A review. *Sci. Atmos. Sin.*, **22**, 1–12.

521 Wang, C.-C., Y.-H. Chen, H.-C. Kuo, S.-Y. Huang, 2013: Sensitivity of typhoon track  
522 to asymmetric latent heating/rainfall induced by Taiwan topography: A numerical  
523 study of Typhoon Fanapi (2010). *Journal of Geophysical Research: Atmospheres*  
524 **118**, 3292-3308.

525 Wang, Y., and G. J. Holland, 1996a: The beta drift of baroclinic vortices. Part I:  
526 Adiabatic vortices. *J. Atmos. Sci.*, **53**, 411–427.

527 Wang, Y., and G. J. Holland, 1996b: The beta drift of baroclinic vortices. Part  
528 II:Diabatic vortices. *J. Atmos. Sci.*, **53**, 3737–3756.

529 Wang, Y., and G. J. Holland, 1996c: Tropical cyclone motion and evolution in vertical  
530 shear. *J. Atmos. Sci.*, **53**, 3313–3332.

531 Willoughby, H., 1988: Linear motion of a shallow-water, barotropic vortex. *J. Atmos.*  
532 *Sci.*, **45**, 1906–1928.



533 Wu, C.-C., and K. A. Emanuel, 1993: Interaction of a baroclinic vortex with  
534 background shear: Application to hurricane movement. *J. Atmos. Sci.*, **50**, 62–76.

535 Wu, C.-C., and K. A. Emanuel, 1995a: Potential vorticity diagnostics of hurricane  
536 movement. Part I: A case study of Hurricane Bob (1991). *Mon. Wea. Rev.*, **123**,  
537 69–92.

538 Wu, C.-C., and K. A. Emanuel, 1995b: Potential vorticity diagnostics of hurricane  
539 movement. Part II: Tropical Storm Ana (1991) and Hurricane Andrew (1992).  
540 *Mon. Wea. Rev.*, **123**, 93–109.

541 Wu, C.-C., Y.-H. Huang, and G.-Y. Lien, 2012: Concentric eyewall formation in  
542 Typhoon Sinlaku (2008) – Part I: Assimilation of T-PARC data based on the  
543 Ensemble Kalman Filter (EnKF). *Mon. Wea. Rev.*, **140**, 506-527.

544 Wu, L., and B. Wang, 2000: A potential vorticity tendency diagnostic approach for  
545 tropical cyclone motion. *Mon. Wea. Rev.*, **128**, 1899-1911.

546 Wu, L., and B. Wang, 2001a: Movement and vertical coupling of adiabatic baroclinic  
547 tropical cyclones. *J. Atmos. Sci.*, **58**, 1801-1814.

548 Wu, L., and B. Wang, 2001b: Effects of convective heating on movement and vertical  
549 coupling of tropical cyclones: A numerical study. *J. Atmos. Sci.*, **58**, 3639-3649.

550 Wu, L., J. Liang, and C.-C. Wu, 2011a: Monsoonal Influence on Typhoon Morakot  
551 (2009). Part I: Observational analysis. *J. Atmos. Sci.*, 2208–2221.

552 Wu, L., H. Zong, and J. Liang, 2011b: Observational analysis of sudden tropical  
553 cyclone track changes in the vicinity of the East China Sea. *J. Atmos. Sci.*, **68**,  
554 3012–3031.

555 Wu, L., S. A. Braun, J. Halverson, and G. Heymsfield, 2006: A numerical study of  
556 Hurricane Erin (2001). Part I: Model verification and storm evolution. *J. Atmos.*  
557 *Sci.*, **63**, 65–86.

558 Yu, H., W. Huang, Y. H. Duan, J. C. L. Chan, P. Y. Chen, R. L. Yu. (2007) A  
559 simulation study on pre-landfall erratic track of typhoon Haitang (2005).  
560 *Meteorology and Atmospheric Physics*, **97**, 189-206.

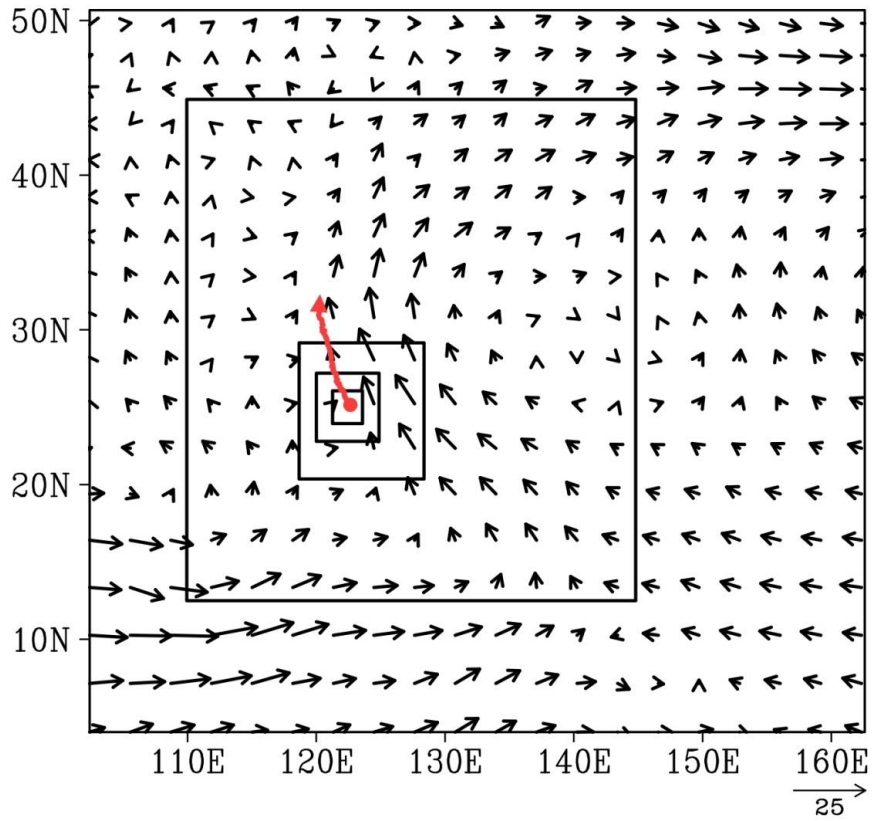
561

562

563

564

565

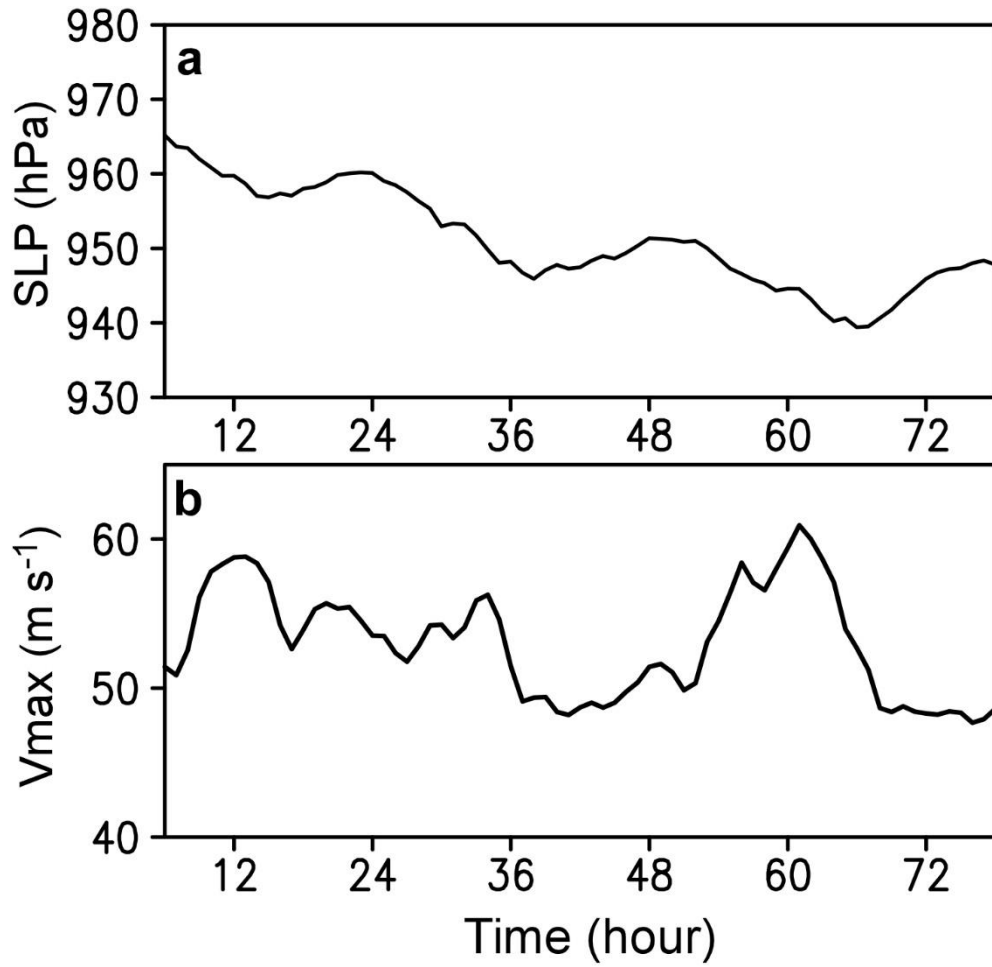


566

567 Figure 1 Model domains of the numerical experiment with the three innermost

568 domains moving with the storm, the initial 850-hPa wind ( $\text{m s}^{-1}$ ) field (vectors), and

569 the simulated tropical cyclone track (red)

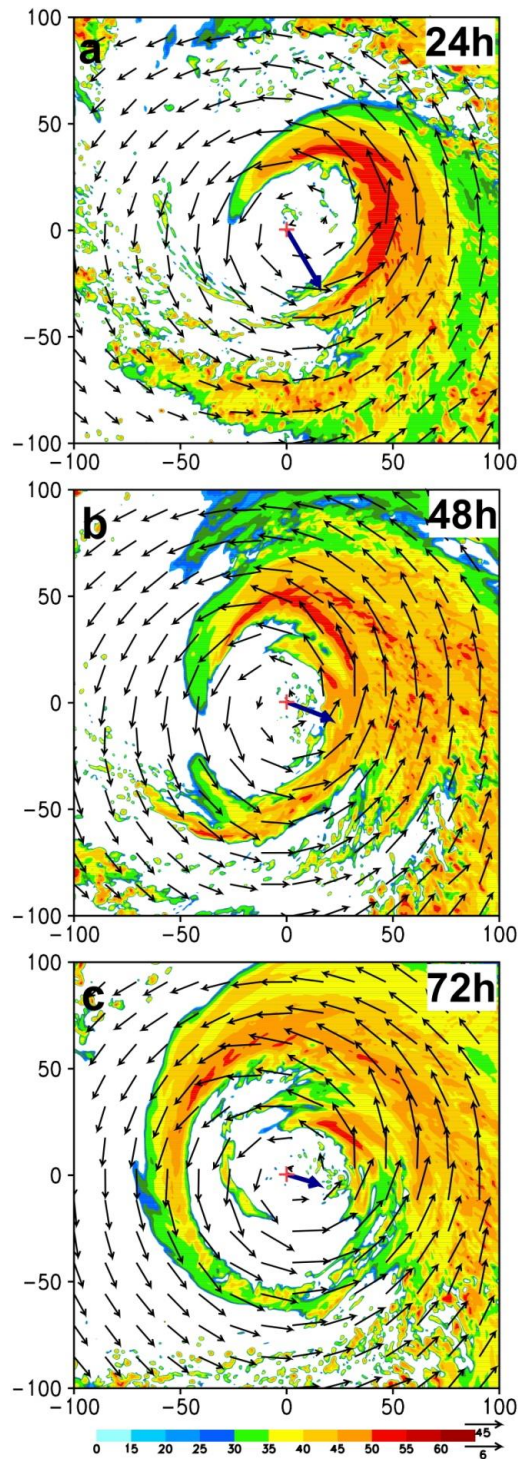


570

571 Figure 2 Time series of tropical cyclone intensity: a) sea level minimum pressure

572 (hPa); b) maximum wind speed at 10 m (m s<sup>-1</sup>).

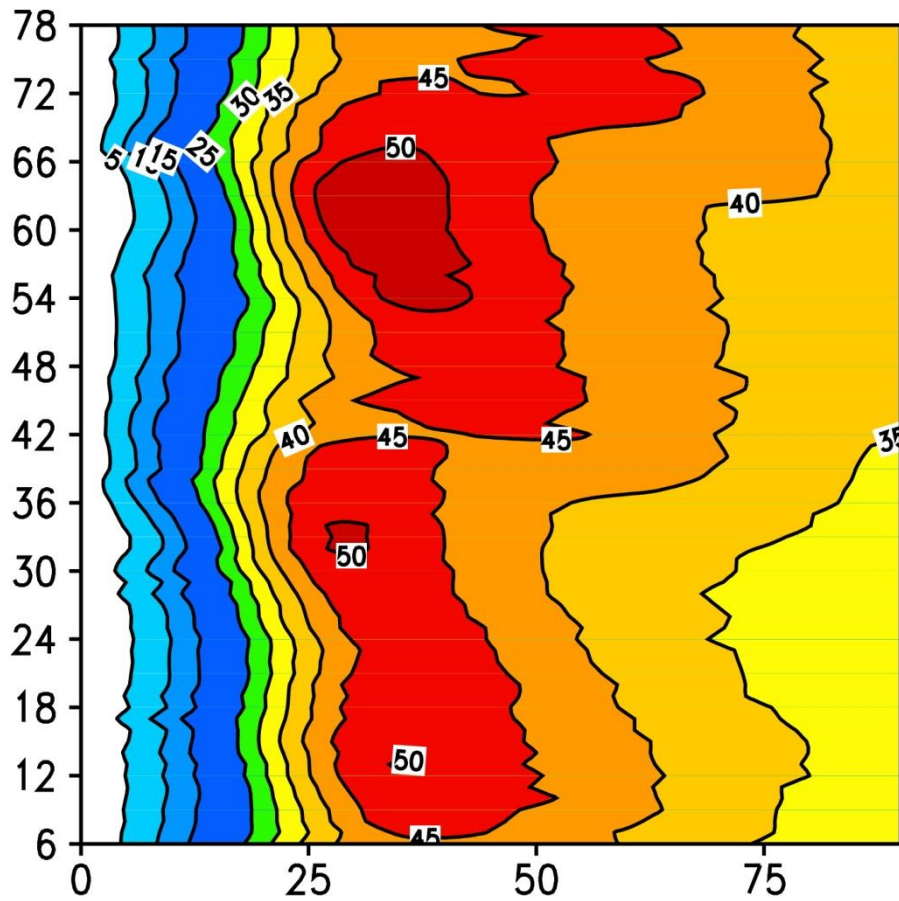
573



574

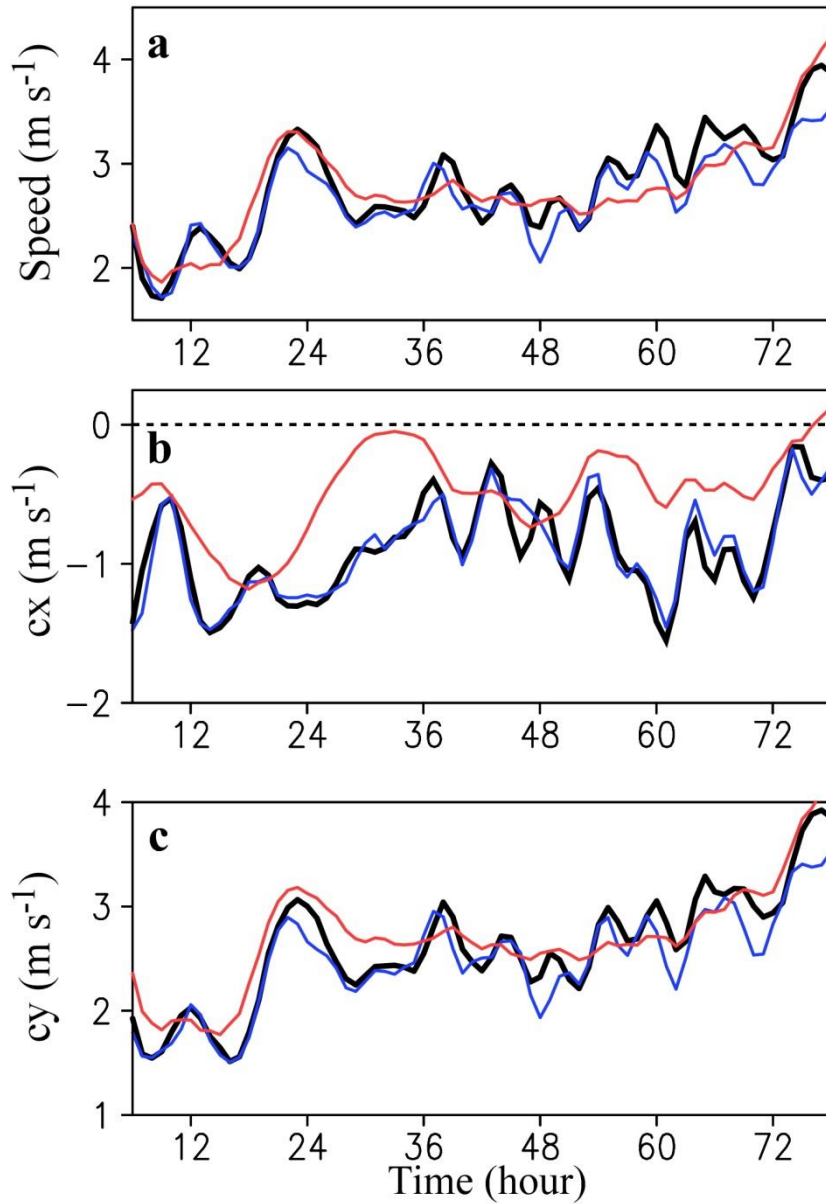
575 Figure 3 Simulated wind (vectors,  $\text{m s}^{-1}$ ), radar reflectivity (shading, dBz) fields at  
 576 700 hPa, and the vertical wind shear (bold arrows in the center) between 200 hPa and  
 577 850 hPa after (a) 24-h, (b) 48-h, and (c) 72-h integration. The x and y axes indicate  
 578 the distance (km) relative to the storm center. The upper (lower) scale vector at the  
 579 right lower corner is for the 700-hPa wind (vertical wind shear).

580



581

582 Figure 4 Evolution of the simulated azimuthal mean component ( $\text{m s}^{-1}$ ) of the 700-hPa  
 583 wind in the 9-km domain. The x-axis and y-axis indicate the distance (km) from the  
 584 storm center and the integration time (hours).



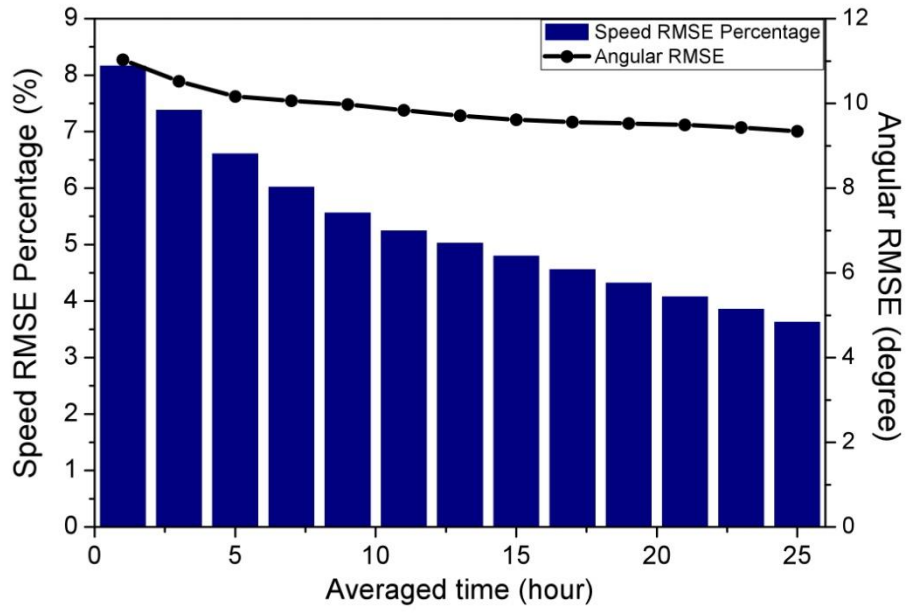
585

586 Figure 5 Time series of tropical cyclone speed (thick black), PVT speed (blue) and

587 conventional steering (red): a) magnitude, b) zonal component, and c) meridional

588 component

589

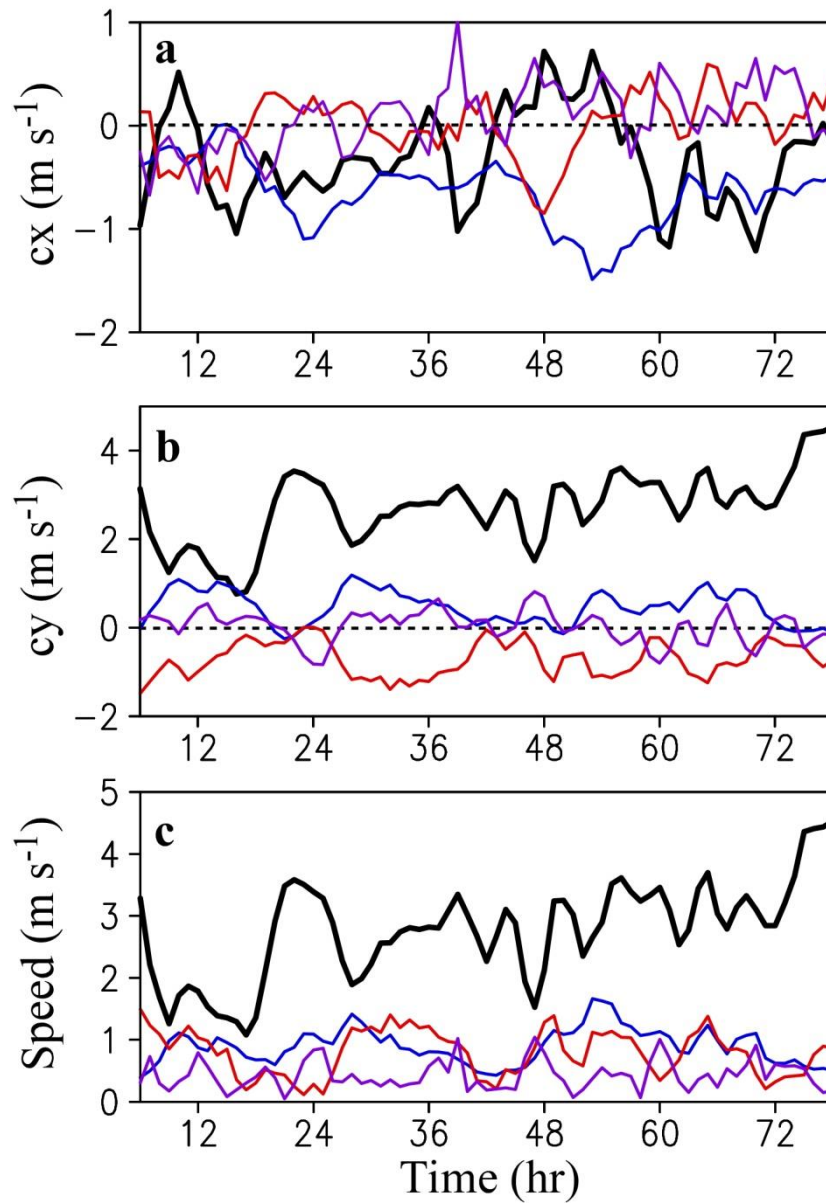


590

591 Figure 6 Changes of the RMSEs of the speed (blue boxes, %) and direction (black

592 dots, °) of the conventional steering averaged over various time periods





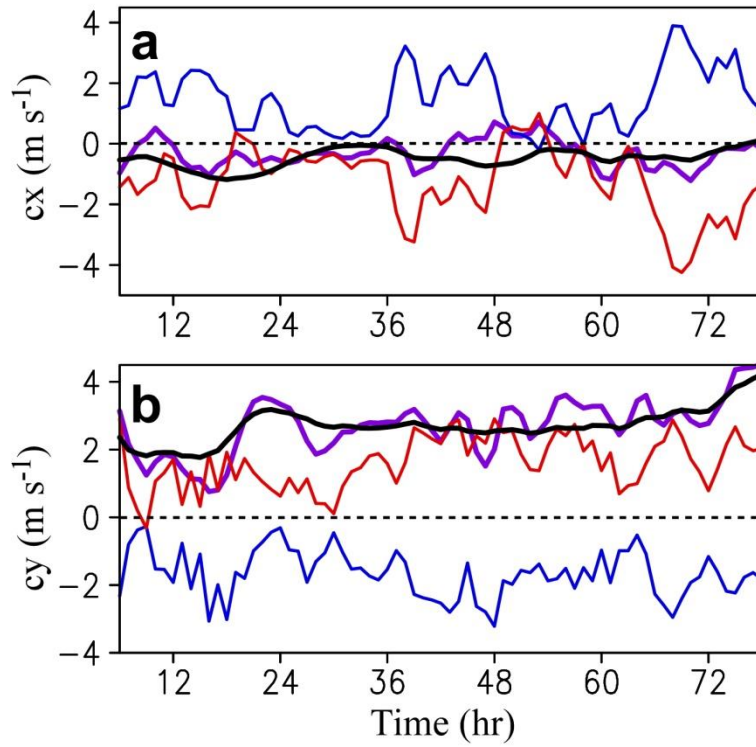
593

594 Figure 7 Contributions of the horizontal advection (HA, black), vertical advection

595 (VA, blue), diabatic heating (DH, red) and friction (FR, purple) terms in the PVT

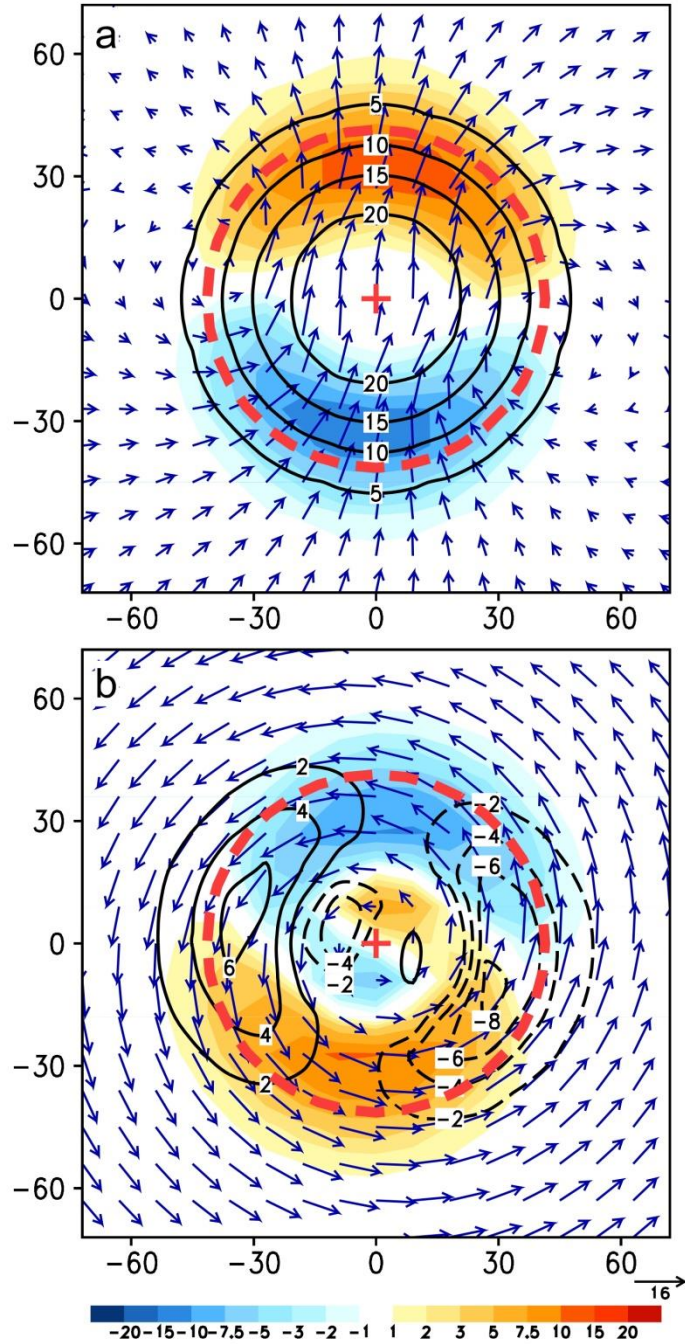
596 equation to tropical cyclone motion: a) zonal component, b) meridional component,

597 and c) magnitude



598

599 Figure 8 Time series of the conventional steering (thick black) and the contributions  
 600 of the HA (thick purple) and the HA1 (red) and HA2 (blue) terms: a) zonal  
 601 component, b) meridional component. Note that the conventional steering is deducted  
 602 from the contribution of the HA1 term.



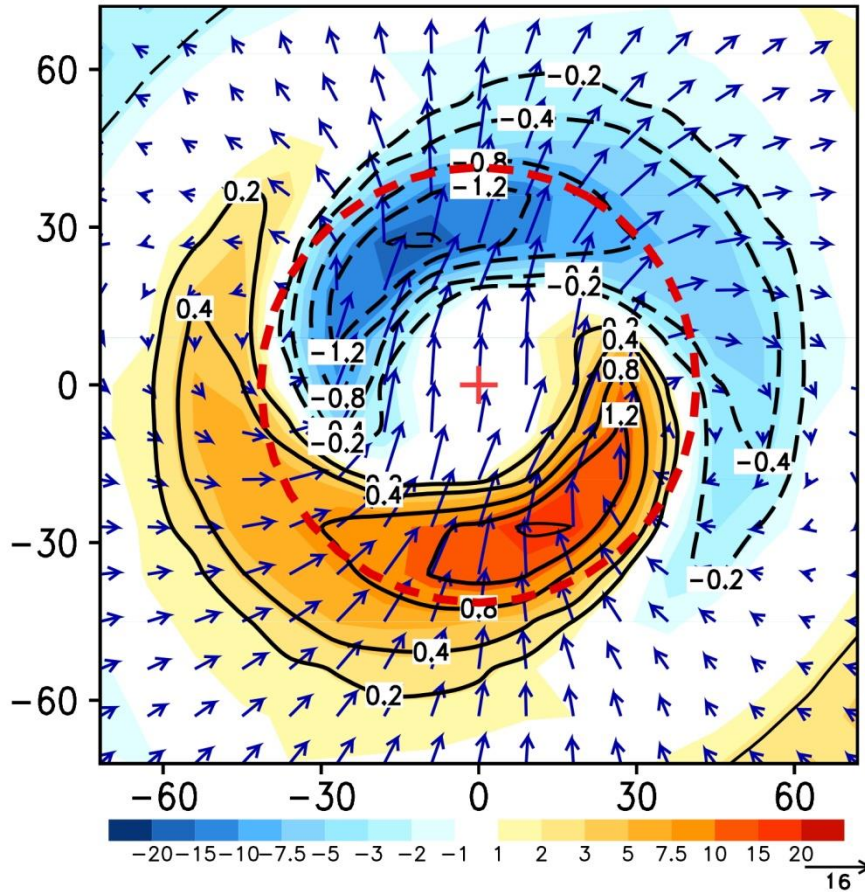
603

604 Figure 9 (a) HA1 (shaded,  $10^{-10} \text{ m}^2 \text{ s}^{-2} \text{ K kg}^{-1}$ ) and (b) HA2 (shaded,  $10^{-10} \text{ m}^2 \text{ s}^{-2} \text{ K}$

605  $\text{kg}^{-1}$ ) with the wavenumber-one and symmetric components of potential vorticity

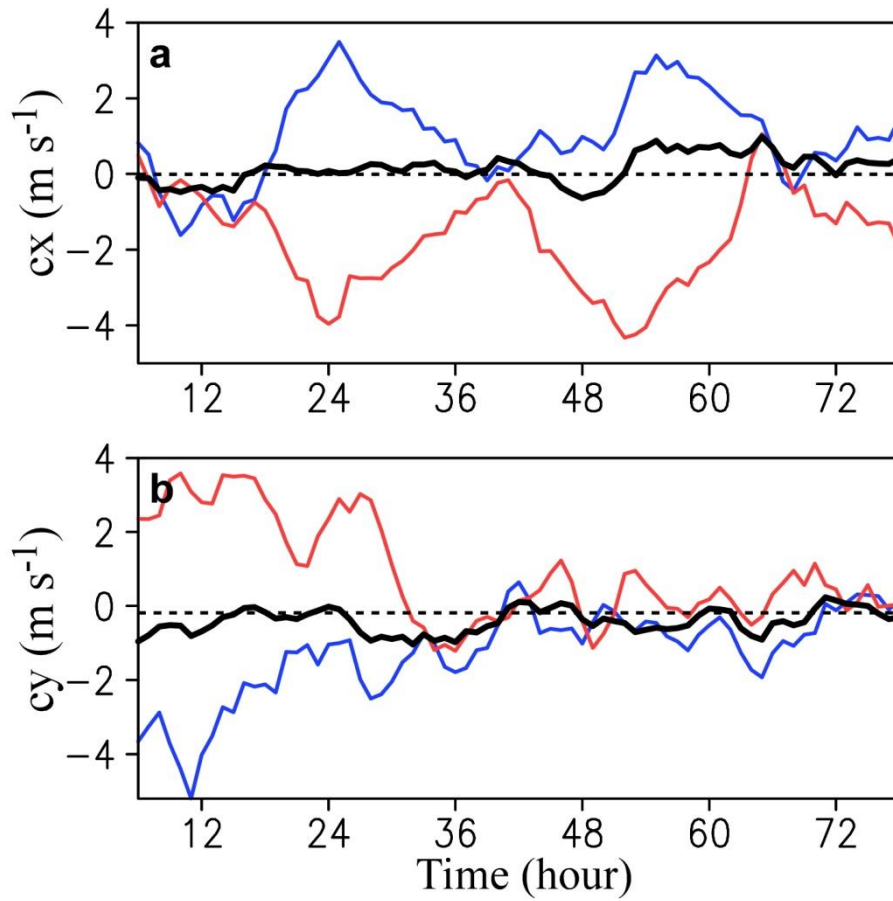
606 (contours,  $10^{-6} \text{ m}^2 \text{ s}^{-1} \text{ K kg}^{-1}$ ) and winds (vectors,  $\text{m s}^{-1}$ ) at 700 hPa after 18 hours of

607 integration. The dashed circle indicates the radius of maximum wind.



608

609 Figure 10 The wavenumber-one components of the 500-hPa vertical motion (contours,  
 610  $\text{m s}^{-1}$ ), 700-hPa winds relative to the tropical cyclone motion (vectors,  $\text{m s}^{-1}$ ), and  
 611 500-hPa heating rate (shaded,  $10^{-4} \text{ K s}^{-1}$ ) after 18 hours of integration. The dashed  
 612 circle indicates the radius of maximum wind.

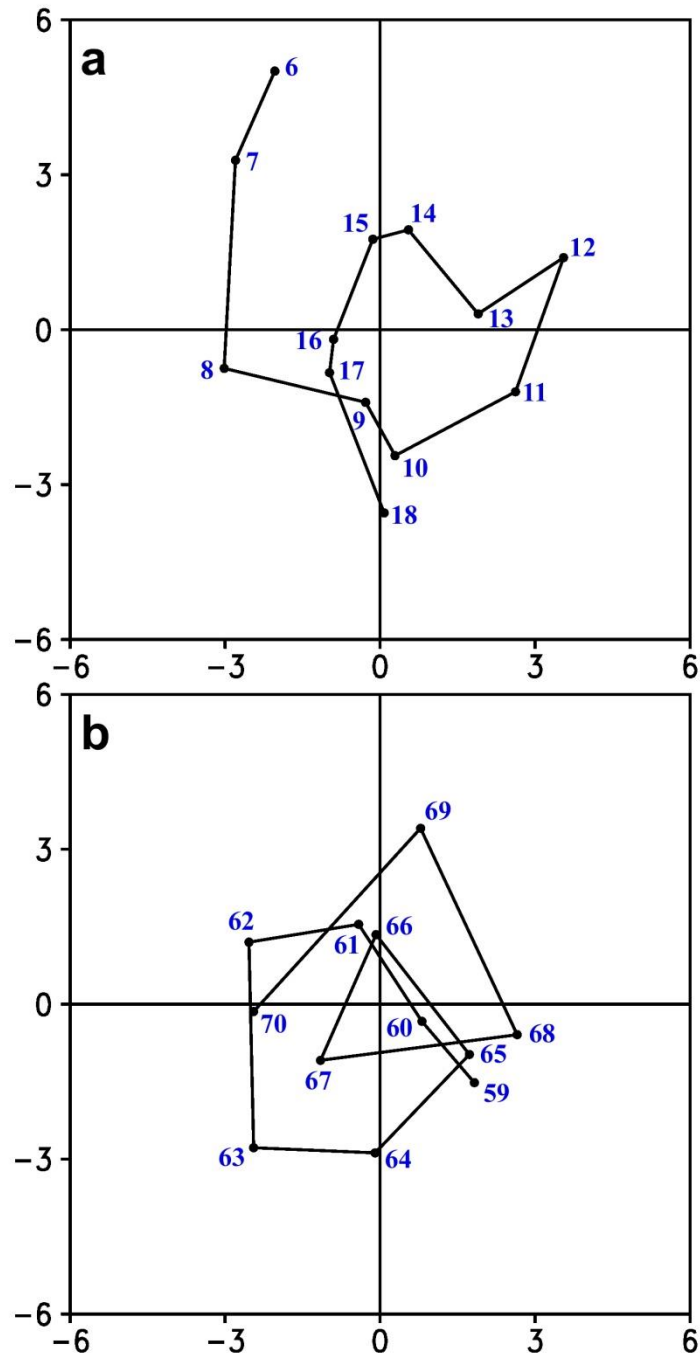


613

614 Figure 11 Time series of the contributions of diabatic heating at 700 hPa (blue) and

615 400 hPa (red) and the contribution of diabatic heating (thick black) averaged over the

616 layer between 300 hPa and 850 hPa



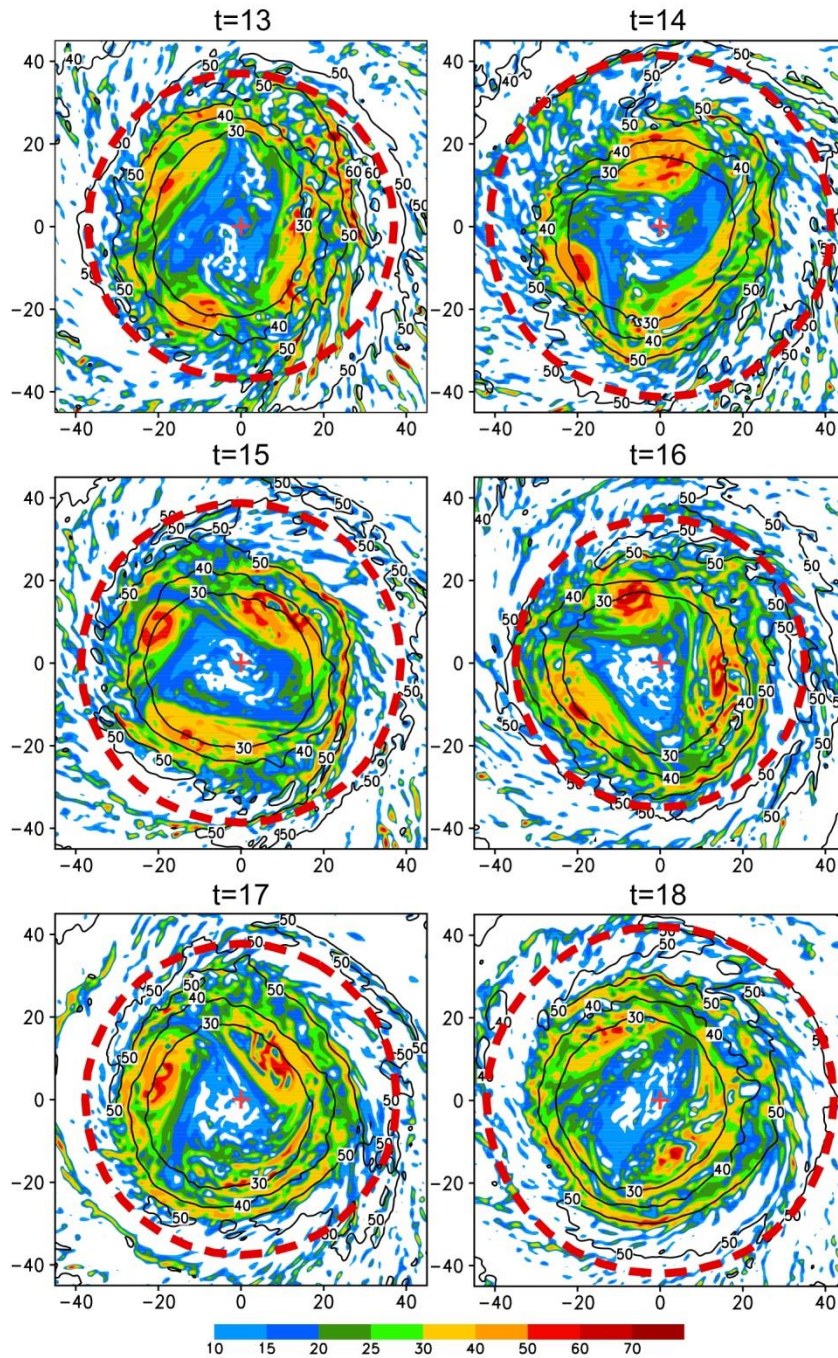
617

618 Figure 12 Small-amplitude oscillation of the tropical cyclone track with respect to the

619 9-hour running mean track: a) 6-18 h and b) 59-69 h. The x and y axes indicate the

620 distance (km) relative to the 9-hour running mean track.

621



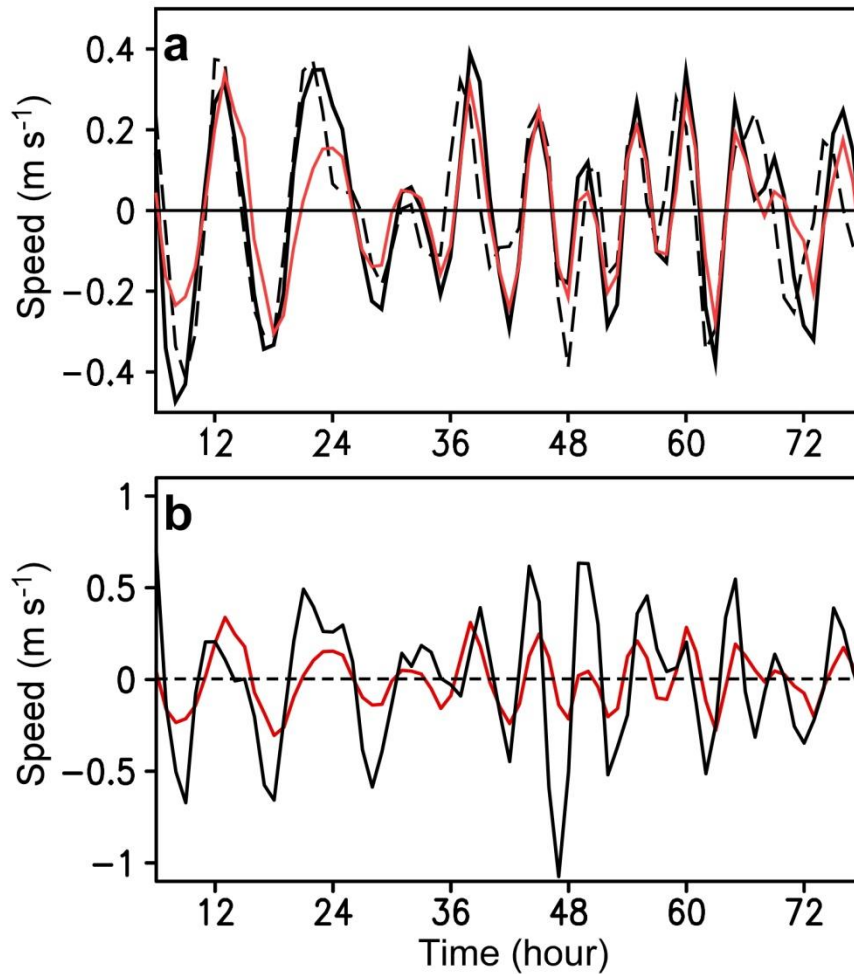
622

623 Figure 13 Distribution of potential vorticity (shaded,  $10^{-6} \text{ m}^2 \text{ s}^{-1} \text{ K kg}^{-1}$ ) and  
 624 magnitude of wind (contour,  $\text{m s}^{-1}$ ) within inner-core region during 13-18 h at 700 hPa.

625 The dashed circle shows the radius of maximum wind with the tropical cyclone center  
 626 indicating with crosses.

627

628



629

630

631 Figure 14 Fluctuations (deviation from the 9-hour running mean) of (a) the tropical

632 cyclone speed (black solid), the PVT speed (black dashed) and the difference between

633 the tropical cyclone speed and the conventional steering (red solid), and (b) the

634 difference between the tropical cyclone speed and the conventional steering (red

635 solid), and the difference between the contribution of the HA term and the

636 conventional steering (black).

637

638